Ceramics, Glass and Glass-Ceramics for Personal Radiation Detectors

Subjects: Physics, Applied

Contributor: Szymon Świontek , Marcin Środa

Different types of ceramics and glass have been extensively investigated due to their application in brachytherapy, radiotherapy, nuclear medicine diagnosis, radioisotope power systems, radiation processing of food, geological and archaeological dating methods. The comparison of the physico-chemical properties shows that glassy materials could be a promising alternative for dosimetry purposes.

thermoluminescence (TL) high energy dose dosimetry

1. Introduction

Thermoluminescent dosimetry is a science which deals with measuring doses of ionizing radiation with the use of TL detectors. Thermoluminescence (TL) dosimetric studies have significant impact on many fields useful in ordinary life such as: radiotherapy [1], nuclear medicine diagnosis [2], radioisotope power systems [3], radiation processing of food [4], geological and archaeological dating methods [5][6], radiation shielding materials [7][8]. Due to the increasing use of ionizing radiation in technology, it seems that we must search for better materials suitable for radiation shielding. The amorphous structure of the glass, which is characterized by exceptional chemical resistance, seems to be ideal for this type of application. Moreover, the thermoluminescent materials are used in measurements of terrestrial and cosmic radiation [9] or radionuclide sources [10]. The phenomenon of thermoluminescence depends on the light emission as a result of heating a sample that was previously exposed to ionizing radiation. The luminescence mechanism in this case can be considered as phosphorescence caused by increasing temperature. The light emission can be observed directly during the first heating process. Luminescence can also be observed again after radiation exposure of a specific wavelength. The phenomenon of thermoluminescence occurs mainly in dielectrics [11] but also in organic materials [12]. The thermoluminescence effect was firstly observed and described in 1663 by the English physicist Robert Boyle [13]. Thermoluminescence was acknowledged in a diamond which had been heated to the temperature of the human body. Then, in 1904 Maria Skłodowska-Curie observed temperature-stimulated luminescence in fluorite (CaF_2) [14]. She noticed the relationship between the exposure of natural calcium fluoride to radium radiation and the intensity of its light emission. The practical application of the thermoluminescence phenomenon in dosimetry was not developed until the end of the first half of the twentieth century, when the Randall-Wilkins theory was formulated [15]. Since the discovery of the phenomenon of thermoluminescence, many monographs and review articles containing the physical basis of this phenomenon have been published. The books “Thermoluminescence and Thermoluminescent Dosimetry”, by Yigal S. Horowitz [16] and “Thermoluminescence of solids” by S.W.S. McKeever

[17], are worth mentioning. In addition, many summary reviews have been written on this subject, such as: “Thermoluminescence dosimetry and its applications in medicine” by T. Kron [18], “Thermoluminescence and its Applications: A Review” by K.V.R. Murthy [19] or “Versatility of thermoluminescence materials and radiation dosimetry—A review” by A. Duragkar [20]. The purpose of the following review article is to summarize the knowledge of the thermoluminescent properties of glassy and glass-crystalline materials.

The vast majority of the analytical methods applied in the glow-curve analysis are based on one recombination and one trapping level. Unfortunately, there is no ideal TL material which can be thoroughly specified by this model. Given the degree of defect centers and arrangement complexity in glassy networks, it is an extremely difficult case to understand the physical principles of thermoluminescent phenomena for amorphous systems. Therefore, the calculated values of activation energy E_A and frequency factors f are, in fact, effective values. The glow curve shape depends on several factors, such as: the TL material composition, kind of dopants, types of defect centers induced by irradiation, the type of ionizing radiation and its dose level. The shape of the TL glow-curve for glassy samples might be explained by the presence of multiple trapping points which increase the probability of re-trapping mechanism. It is widely understood that the shape factor of a standard first order peak is about equal to 0.42 [21]. Simultaneously, when the value of shape factor is greater than 0.52, we are dealing with second order kinetics mechanism, respectively. Moreover, it has been demonstrated that the various heating rates can affect on TL glow-curve shape along with different values of trapping parameters [22]. In general, with the increasing heating rate, the TL peak temperature shifts to higher temperatures region. The increase in the intensity of thermoluminescence signal with respect to a radiation dose is caused by increasing number of excited electrons. The standard shape and position of glow TL peaks can be changed in respect to location of trapping levels in the glassy network [23]. Primarily, when the shape of the glow curve is asymmetric, wider at the low temperature region than at the high temperature region, then the kinetic process of thermoluminescence is attributed to the first order [24]. It can be equivocally expressed as no re-trapping luminescence process during which all the charge carriers freed from the trap centers follow directly to the recombination points. The thermally stimulated luminescence (TL) can be used to determine the optic properties of the glasses under study with radiation doses [25].

The process of irradiation might induce the displacement of atoms or electron defects which include the changes in the valence state of network atoms, modifier, or impurity atoms. Moreover, the changes in the glow curve shape can be used to deduce the damage created by the high radiation to the thermoluminescent material [26]. The extent of disordering in glass network can be deduced from Urbach energy (Urbach tail) which described the localized states present in the bandgap [27]. During irradiation, atoms are ionized as the bound electrons interact with high energy particles. This interaction leads to the generation of electron-hole pairs which got trapped at structure defects or glass impurities having energy states within the forbidden band. As a result of this ionization process, the electron-hole pairs in the glass structure are generated after exposing to ionizing radiation. In the case of borate and phosphate glasses, radiation defects are related mainly to the absence or excess of oxygen atoms in the amorphous glass structure [28][29][30]. For silicate, telluride or heavy metal fluoride glasses, radiation defects may be also color centers or structural vacancies [31][32]. Therefore, when heat or light stimulate the structure of the glass, the recombination of charges results in luminescence.

2. The parallel of highest phonon energy and ultraviolet cut-off wavelength in different glass systems.

The thermoluminescent detector was used in ionizing radiation dosimetry for the first time during nuclear testing as part of the Manhattan Project in the United States since 1942 [33]. Nowadays, we are observing a tremendous progress in the thermoluminescence dosimetry from that moment [34][35][36][37]. The most commonly used material in TL detectors is crystalline lithium fluoride. There are a several types of detectors based on this compound: MCP detector (LiF doped Mg, Cu and P), MTS detector (LiF doped Mg and Ti) or MTT detector (LiF doped Mg and Ti with ten times more titanium and almost three times less magnesium in comparison with the MTS detector) [38]. The most important advantages of these detectors are high sensitivity and a cross-section for interaction with ionizing radiation which are similar to that of human tissues. Natural lithium contains 92.5% of the ^{7}Li isotope and 7.5% of the ^{6}Li isotope. The TL detectors also use lithium depleted or enriched in the ^{6}Li isotope, which corresponds to three subtypes: MCP-N (natural abundance of lithium isotopes), MCP-6 (^{6}Li-enriched) and MCP-7 (^{7}Li-enriched) [39]. MTS-N detectors are characterized by a linear thermoluminescence response to approx. 1 Gy, and the reduction in the signal at room temperature is estimated at several percent per year. Moreover, they are characterized by good tissue similarity, therefore they are used in environmental and individual dosimetry. The MCP-N detector is characterized by thirty times greater sensitivity than the MTS-N detector and three times lower own background. This allows the measurement of radiation doses at the level of 200 nGy, which is a result 100 times lower in comparison with the MTS-N detector. The response of the MCP-N detector is linear up to a few Gy and has good stability over time. The spontaneous decrease in the stored radiation signal over time amounts to approx. 5% per year in the room temperature. The MTT-N detector is more efficient than the MTS-N detector, but its sensitivity is approximately 2.5 times lower. Therefore, the minimum measured dose is 1 mGy.

Fluorides and calcium sulphates doped Tm or Dy and Al_2O_3 doped carbon are also successfully used as thermoluminescent materials [40][41]. However, in practice, they are less often used items than crystalline doped LiF due to the different cross-section for interaction with radiation in comparison with human tissues. The most important technical parameters that prove the quality of thermoluminescent materials include: a wide range of energy of the measured doses, the linearity of the response to the radiation dose, potentially small geometric dimensions, the lack of need for power supply and chemical resistance to environmental factors. An undesirable feature of the thermoluminescent material is the high annealing temperature during the dose reading procedure. Thermoluminescent detectors are usually in the form of sintered bulk ceramics or powders. The most commonly used TL detectors are based on the doped: LiF, Al_2O_3, CaF_2 and $CaSO_4$ [40][41][42]. The comparison of the thermoluminescence glow curves for the same radiation dose for the crystalline TL materials is presented in the **Figure 1**.

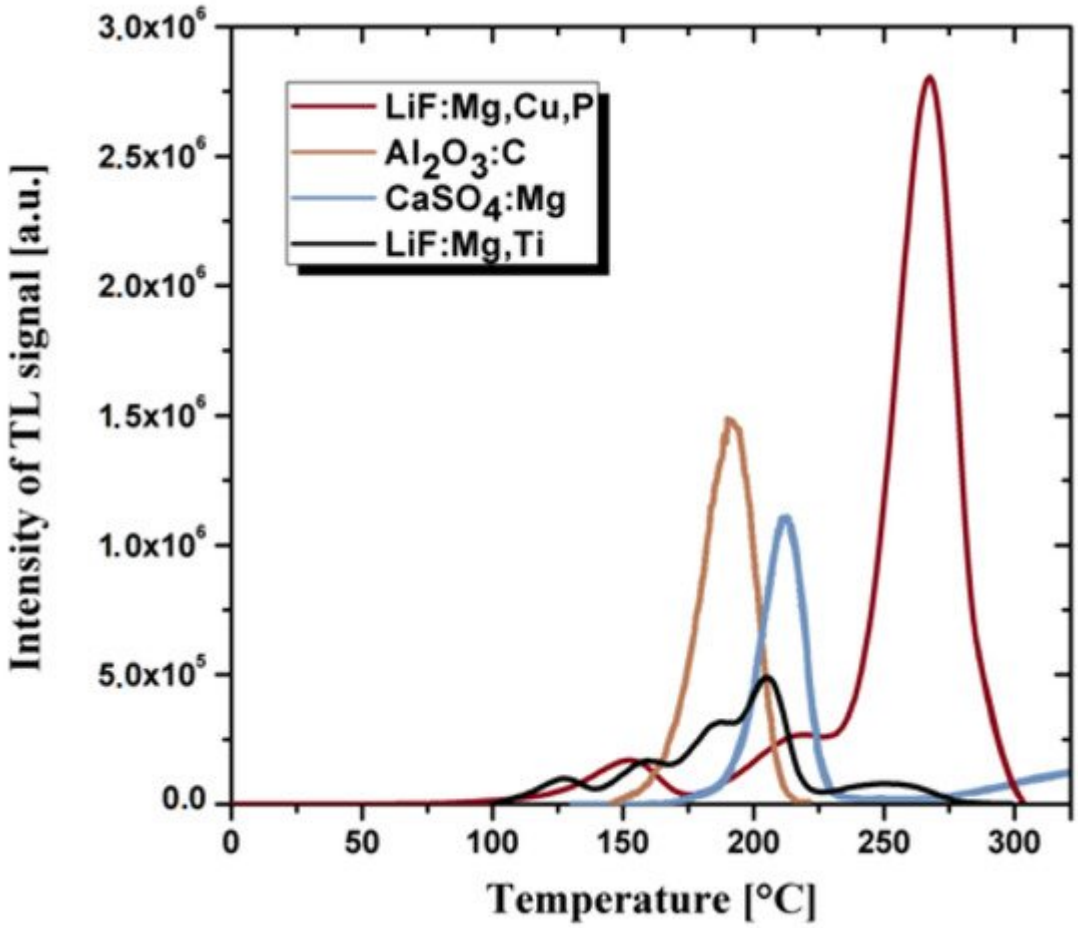

Figure 1. The comparison of the thermoluminescence glow curves for various crystalline materials used commercially as TL detectors after 10 mGy radiation dose. Data collected from the publications [38][41][42].

The glass matrix with optically active dopants may also be of interest for developing dosimetric detectors. The borate glasses have a high transparency and high solubility for the rare-earth ions among other oxide glasses, i.e., silicates, phosphates and tellurite glasses [43]. However, due to their multiple phases, high phonon energy and low moisture resistance, borate glasses have some limitations to their optical gain medium. On the other hand, the borosilicate glasses have a better thermal stability, higher value of refractive index and lower dispersion as well as higher chemical resistance [44]. Therefore, these glasses are widely used for optoelectronics [45] and optical lenses applications [46] and also as glass cookware due to low thermal expansion coefficient [47]. The incorporation of rare-earth elements to the glass matrix can induce thermoluminescence effect and produce optical active materials [48]. These dopants act as luminescent centers what enables radiation processes.

The incorporation of alkali ions in the borate network can reduce the risk of different phases formation in the glass by converting BO_3 triangle borate units to BO_4 tetrahedra [49]. The addition of fluoride ions to oxide glasses induces the special oxyfluoride properties which combine the low phonon energy and value of refractive index of fluorides with thermal stability towards devitrification of the oxide glasses. For example, after incorporation of lithium ions to borate glass network, the negative charge of the boron-oxygen tetrahedron is compensated by lithium cations [50]. Moreover, alkali fluoride (i.e., LiF, KF or NaF) can be introduced to borate network up to 45 mol%. The

rearrangement of lithium ions due to its small radius can likewise be caused by irradiation or glass matrix imperfection. Therefore, it enables formation of negative point defects which play a role of hole traps. On the other hand, oxygen vacancy formed a positive point defect which play a role of electron traps. That explains why, after lithium oxide addition to borate matrix, boron-oxygen triangle attaches an additional oxygen atom forming boron-oxygen tetrahedron. The oxyfluoride glasses from the LiF-B_2O_3-SiO_2 system are characterized by favorable thermoluminescent properties [51]. The increase in lithium fluoride contribution from 20 to 40 mol% in the borosilicate glass causes efficiency enhancement of the thermoluminescence signal. Moreover, the process of controlled crystallization based on DSC curves can increase TL sensitivity, narrowing and shifting the main TL peak to the lower temperatures. The glass-ceramics with 40 mol% LiF containing $LiBF_4$ optically active phase exhibits similar level of TL signal to commercially used doped LiF materials [52].

The addition of a heavy metal oxide to the borate network increases the transmission of light in the mid-infrared region and decreases the melting temperature and the phonon energy [53]. Alkali-heavy metal oxide borate glasses show high UV–vis–NIR transparency, low melting and glass transition temperatures, low phonon energy, low thermal expansion coefficient, good mechanical strength and chemical stability [54]. Among various glass hosts, a borate matrix is a proven good radiation absorber with a cheap processing [55]. The effective atomic number Z_{eff} of network former B_2O_3 is about 7.35 which is close to that of human tissue (Z_{eff} = 7.42) [56]. Heavy metal oxides, such as BaO, decrease the phonon energy of the glass matrix, and simultaneously increase the efficiency of luminescence [57]. It has been observed that the addition of BaO up to 25 mol% to borate glass could help improve the thermoluminescence intensity.

In some cases, commercial borate glasses exhibit UV charge transfer absorption because of the trace iron impurities presence (largely Fe^{3+} ions) [58]. It was proved that transition metal (TM) ions even for the ppm level in glasses could produce strong UV absorption. Moreover, the charge transfer mechanism for glasses has been thoroughly classified based on trace transition metal impurities content (such as Fe^{3+} or Cr^{6+}) [59]. The increased absorption in the range of ultraviolet results from an electron transfer mechanism (electron transition from the orbital of a coordinating oxygen atom to an orbital of the metal ion). Abdelghany and ElBatal have observed charge transfer absorption bands in the UV range for a various undoped borate glasses [60][61]. Therefore, the trace iron impurities (largely Fe^{3+} ions) which are present in the chemical reagents/raw materials can induce UV absorption mechanisms in different glass systems.

P_2O_5 is often used in the optically active glasses due to the shift of the absorption cut-off wavelength to the near infrared region (NIR) [62][63]. The advantage of phosphate glass is its higher solubility of rare earths in its structure in comparison with silicate glasses. Moreover, the lithium fluoride added to phosphate glass causes a decrease in thermal fading at the room temperature [64]. Rare-earth ions, in their trivalent state, act as fluorescence activators when doped in the phosphate glass matrix and enhance TL emission. However, photo and thermoluminescence properties of the RE ions are sensitive to various solid-state hosts. They exhibit absorption bands in the near-UV to blue region and sharp emission bands in the entire visible region of the electromagnetic spectrum, which is expected for visible solid-state lasers and light emitting diodes [65]. The amorphous nature of the glasses makes them susceptible to accommodate radiation-induced defects what is also their advantage.

Pure phosphate glasses produce no TL signals [66]. However, lithium-doped phosphate glasses characterize a broad TL peak at the rage of 200–300 °C [67]. On the other hand, barium-doped phosphate glasses feature at least two TL peaks, approximately at 220 and 390 °C, which are attributed to Ba^{2+} ions [68]. The observed TL peaks result from various defects generated by the modifier ions (Ba^{2+} and Li^{+}) inserted into the glass matrix. The low temperature peak characterizes an average intensity loss of 57% after 2 days of storage and a reduction to 9% of the initial signal after 4 months of storage. Thus, thermal fading makes using this peak for dosimetry purposes difficult. The high temperature peak also fades in the short term, but it eventually stabilizes at 75% of the initial value [69]. They also give a fast-decaying OSL signal correlated with the low temperature of TL peak. The optically stimulated luminescence signal increases linearly with the received dose for phosphate glasses containing both barium and lithium ions [70]. On the other hand, a 100-h delay readout after irradiation shows the signal decrease to less than 50% of the initial dose value. The content of barium ions Ba^{2+} allows linear characteristics of the dose response in phosphate glasses up to 100 Gy. Moreover, phosphate glass doped with barium oxide is at least one order of magnitude more sensitive to radiation than the glass doped with lithium oxides [71].

The article presents the thermoluminescent properties of mainly borate and phosphate glasses due to the similar cross-section on the interaction with ionizing radiation to human tissues [72][73]. Unfortunately, silicate and telluride glasses have Z_{eff} significantly different than most human organs [74][75]. For this reason, the use of these materials in personal dosimetry is very difficult.

Another group are fluoride glasses, the development of which was initiated by the discovery of the glass-forming properties of zirconium fluoride—ZrF_4. These glasses are based on heavy metal fluoride glasses (HMFG) and are characterized by—compared to oxide glasses—low attenuation of signals in the infrared range (up to approx. 3 µm). At the same time, fluoride glasses readily accept rare-earth elements into their structure, which makes it possible to use them as optical amplifiers in telecommunications bands operating in the near infrared. **Figure 2** shows the values of the highest phonon energy together with ultraviolet cut-off wavelength in various glass systems.

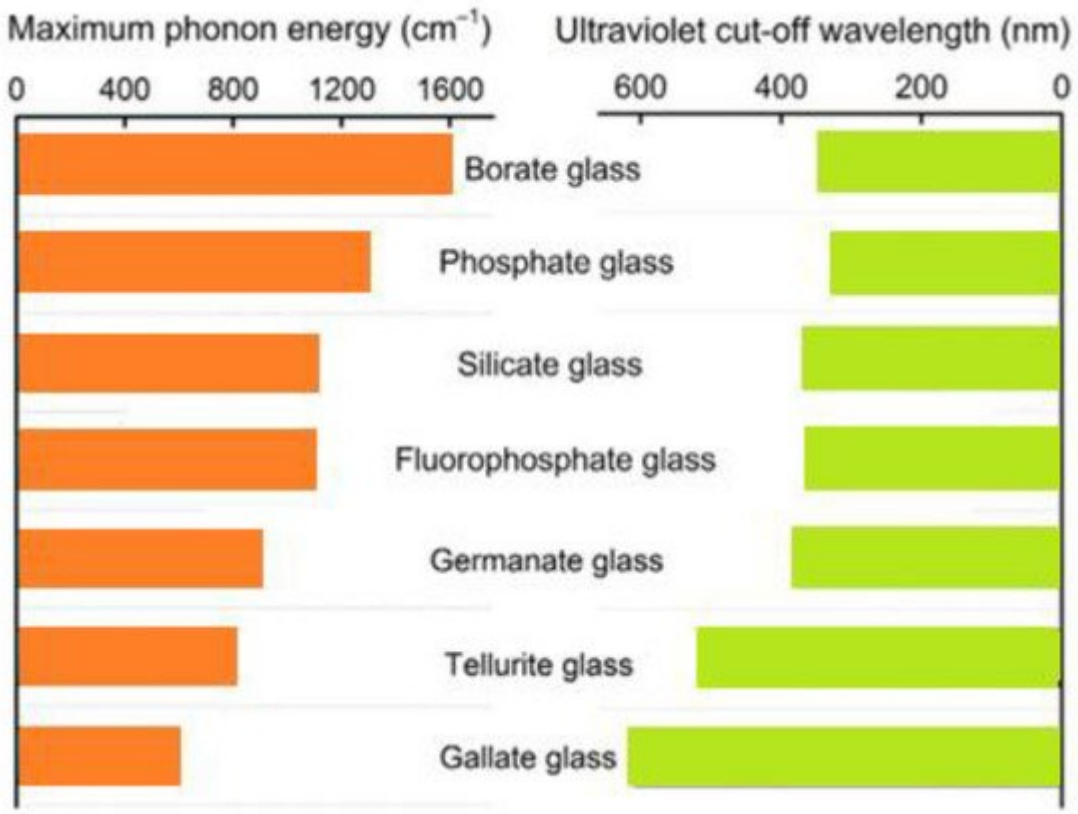

Figure 2. The parallel of highest phonon energy and ultraviolet cut-off wavelength in different glass systems.

References

1. Noor, N.M.; Fadzil, M.S.A.; Ung, N.; Maah, M.; Mahdiraji, G.; Abdul-Rashid, H.; Bradley, D.; Abdul-Rashid, H. Radiotherapy dosimetry and the thermoluminescence characteristics of Ge-doped fibres of differing germanium dopant concentration and outer diameter. Radiat. Phys. Chem. 2016, 126, 56–61.
2. Rivera, T. Thermoluminescence in medical dosimetry. Appl. Radiat. Isot. 2012, 71, 30–34.
3. Pinto, T.N.O.; Antonio, P.L.; Caldas, L.V.E. Measuring TL and OSL of beta radioisotopes inside a glove box at a radiopharmacy laboratory. Radiat. Meas. 2011, 46, 1847–1850.
4. Miyahara, M.M.; Sugi, E.; Katoh, T.; Hironiwa, T.; Sunaga, H.; Luo, L.Z. Study of effective factors in detection of irradiated food using thermoluminescence based on the models of reference minerals. Radiat. Phys. Chem. 2012, 81, 705–711.
5. Sears, D.W.; Sears, H.; Sehlke, A.; Hughes, S.S. Induced thermoluminescence as a method for dating recent volcanism. J. Volcanol. Geotherm. Res. 2018, 349, 74–82.
6. Quickert, N.A.; Godfrey-Smith, D.I.; Casey, J.L. Optical and thermoluminescence dating of Middle Stone Age and Kintampo bearingsediments at Birimi, a multi-component archaeological site in Ghana. Quat. Sci. Rev. 2003, 22, 1291–1297.

7. Mhareb, M.H.A.; Alsharhan, R.; Sayyed, M.I. The impact of TeO2 on physical, structural, optical and radiation shielding features for borate glass samples. Optik 2021, 247, 167924.
8. Dwaikat, N.; Sayyed, M.I.; Mhareb, M.H.A. Durability, optical and radiation shielding properties for new series of boro-tellurite glass. Optik 2021, 245, 167667.
9. Atri, D.; Melott, A.L. Cosmic rays and terrestrial life: A brief review. Astropart. Phys. 2014, 53, 186–190.
10. Niazi, A.; Khabaz, R. An approach to determination of dosimetric characteristics of radionuclide neutron sources with specific constants and effective quality factors. Radiat. Phys. Chem. 2021, 179, 109242.
11. Daneshvar, H.; Shafaei, M.; Manouchehri, F.; Kakaei, S.; Ziaie, F. Influence of morphology and chemical processes on thermoluminescence response. J. Lumin. 2020, 219, 116906.
12. Sugakov, V.; Ostapenko, N.; Ostapenko, Y.; Kerita, O.; Strelchuk, V.; Kolomys, O. Molecular vibrations, activation energies of trapped carriers and additional structure in thermoluminescence of organic polymers. Synth. Met. 2017, 234, 117–124.
13. Cairns, T. Archaeological dating. Anal. Chem. 1976, 48, 267–280.
14. Topaksu, M.; Yazici, A.N. The thermoluminescence properties of natural CaF2 after β-irradiation. Nucl. Instrum. Methods 2007, 264, 293–301.
15. Bos, A.J.J. Theory of thermoluminescence. Radiat. Meas. 2007, 41, 45–56.
16. Horowitz, Y.S. Thermoluminescence and Thermoluminescent Dosimetry; CRC Press Taylor & Francis Group: Boca Raton, FL, USA, 2019.
17. McKeever, S.W.S. Thermoluminescence of Solids. In Cambridge Solid State Science Serie; Cambridge University Press: Cambridge, UK, 1988.
18. Kron, T. Thermoluminescence dosimetry and its applications in medicine. Phys. Eng. Sci. Med. 1994, 17, 175–199.
19. Murthy, K.V.R. Thermoluminescence and its Applications: A Review. Defect Diffus. Forum 2013, 347, 35–73.
20. Duragkar, A.; Muley, A.; Pawar, N.R. Versatility of thermoluminescence materials and radiation dosimetry—A review. Luminescence 2019, 34, 656–665.
21. Kadam, A.R.; Mishra, G.C.; Dhoble, S.J. Thermoluminescence study and evaluation of trapping parameters CaTiO3: RE (RE = Eu3+, Dy3+) phosphor for TLD applications. J. Mol. Struct. 2021, 1225, 129129.
22. Delice, S.; Isik, M.; Gasanly, N.M. Effect of heating rate on thermoluminescence characteristics of Y2O3 nanoparticles. J. Lumin. 2019, 212, 233–237.

23. Bilski, P.; Obryk, B.; Gieszczyk, W.; Baran, P. Position of LiF: Mg, Cu, P TL peak as an alternative method for ultra-high-dose dosimetry. Radiat. Meas. 2020, 139, 106486.
24. Kayacan, O.; Can, N. A generalized method for handling first- and second-order thermal desorption and thermoluminescence. Chem. Phys. 2004, 298, 273–278.
25. Sholom, S.; McKeever, S.W.S.; Chandler, J.R. OSL dosimetry with protective glasses of modern smartphones: A fiber-optic, non-destructive approach. Radiat. Meas. 2020, 136, 106382.
26. Bao, L.; Zha, G.; Gu, Y.; Jie, W. Study on radiation damage effects on CdZnTe detectors under 3 MeV and 2.08 GeV Kr ion irradiation. Mater. Sci. Semicond. Process. 2021, 121, 105369.
27. Tsu, D.V.; Schuelke, T.; Slagter, J. Optical measure of disorder: Why Urbach analysis works for amorphous silicon but fails for amorphous carbon. Diam. Relat. Mater. 2020, 110, 108137.
28. Skuja, L.; Kajihara, K.; Hirano, M.; Hosono, H. Oxygen-excess-related point defects in glassy/amorphous SiO2 and related materials. Nucl. Instrum. Methods Phys. Res. B 2012, 286, 159–168.
29. Elsts, E.; Rogulis, U.; Bulindzs, K. Studies of radiation defects in cerium, europium and terbium activated oxyfluoride glasses and glass ceramics. Opt. Mater. 2015, 41, 90–93.
30. Uklein, A.V.; Popov, A.S.; Lisnyak, V.V. Probing of the oxygen-related defects response in Nd: Phosphate glass within self-action of the laser radiation technique. J. Non-Cryst. Solids 2018, 498, 244–251.
31. Ma, Y.; Su, H.; Zhang, Z. Effect of melting atmospheres on the optical property of radiation-hard fluorophosphate glass. Ceram. Int. 2021, 47, 22468–22477.
32. Lu, Y.; Li, P.; Xie, W. Negative thermal quenching CsPbBr3 glass-ceramic based on intrinsic radiation and vacancy defect co-induced dual-emission. J. Eur. Ceram. Soc. 2021, 41, 3635–3642.
33. Hamzelou, J. The Manhattan memory project. New Sci. 2011, 211, 6–7.
34. Parisi, A.; de Freitas Nascimento, L.; Van Hoey, O.; Mégret, P.; Kitamura, H.; Kodaira, S.; Vanhavere, F. Low temperature thermoluminescence anomaly of LiF: Mg, Cu, P radiation detectors exposed to 1H and 4He ions. Radiat. Meas. 2018, 119, 155–165.
35. Schwahofer, A.; Feist, H.; Georg, H.; Häring, P.; Schlegel, W. Experimental determination of the photon-energy dependent dose-to-water response of TLD600 and TLD700 (LiF: Mg, Ti) thermoluminescence detectors. Z. Für Med. Phys. 2017, 27, 13–20.
36. Iwan, A.; Bilski, P.; KŁosowski, M. Thermoluminescence measurements of liquid crystal azomethines and poly(azomethines) with different shapes as thermo-detectors. J. Lumin. 2010, 130, 2362–2367.

37. Olko, P. Microdosimetry, track structure and the response of thermoluminescence detectors. Radiat. Meas. 2006, 41, 57–70.
38. Parisi, A.; Dabin, J.; Schoonjans, W.; Van Hoey, O.; Mégret, P.; Vanhavere, F. Photon energy response of LiF:Mg,Ti (MTS) and LiF:Mg,Cu,P (MCP) thermoluminescent detectors: Experimental measurements and microdosimetric modeling. Radiat. Phys. Chem. 2019, 163, 67–73.
39. Parisi, A.; Struelens, L.; Vanhavere, F. The relative efficiency of 7LiF:Mg,Ti (MTS-7) and 7LiF:Mg,Cu,P (MCP-7) thermoluminescent detectors for muons, pions and kaons over a broad energy range (2 keV–1 GeV): Theoretical calculations using the Microdosimetric d(z) Model. Radiat. Phys. Chem. 2020, 177, 109096.
40. Hernández, A.; Cruz-Zaragoza, E.; Negrón-Mendoza, A.; Ramos-Bernal, S. Dependence of thermo-luminescence response of calcium sulphate activated by dysprosium on the temperature irradiation. Radiat. Meas. 2004, 38, 431–433.
41. Chithambo, M.L.; Seneza, C.; Kalita, J.M. Phototransferred thermoluminescence of α-Al2O3:C: Experimental results and empirical models. Radiat. Meas. 2017, 105, 7–16.
42. Guckan, V.; Ozdemir, A.; Altunal, V.; Yegingil, I. Studies of blue light induced phototransferred thermoluminescence in CaSO4:Mg. Nucl. Instrum. Nucl. Instrum. Methods Phys. Res. B 2019, 448, 31–38.
43. Rammah, Y.S.; Ali, A.A.; El-Mallawany, R.; El-Agawany, F. Fabrication, physical, optical characteristics and gamma-ray competence of novel bismo-borate glasses doped with Yb2O3 rare earth. Phys. B Phys. Condens. Matter 2020, 583, 412055.
44. Qian, Q.; Zhao, C.; Yang, G.; Yang, Z.; Zhang, Q.; Jiang, Z. Thermal stability and spectroscopic properties of Er3+-doped antimony-borosilicate glasses. Spectrochim. Acta Part A Mol. Biomol. Spectrosc. 2008, 71, 280–285.
45. Tayal, Y.; Rao, A.S. Orange color emitting Sm3+ ions doped borosilicate glasses for optoelectronic device applications. Opt. Mater. 2020, 107, 110070.
46. Pan, L.; Daguano, J.K.; Trindade, N.M.; Cerruti, M.; Zanotto, E.D.; Jacobsohn, L.G. Scintillation, luminescence and optical properties of Ce-Doped borosilicate glasses. Opt. Mater. 2020, 104, 109847.
47. Hasanuzzaman, M.; Rafferty, A.; Sajjia, M.; Olabi, A.G. Properties of Glass Materials. Ref. Modul. Mater. Sci. Mater. Eng. 2016, 1–12.
48. Saidu, A.; Wagiran, H.; Saeed, M.; Obayes, H.; Bala, A.; Usman, F. Thermoluminescence response of rare earth activated zinc lithium borate glass. Radiat. Phys. Chem. 2018, 144, 413–418.

49. Zhu, D.; Ray, C.S.; Luo, F.; Zhou, W.; Day, D.E. Melting and phase-separation of lead borate glasses in low gravity drop shaft. Ceram. Int. 2008, 34, 417–420.
50. Yadav, A.; Dahiya, M.S.; Narwal, P.; Hooda, A.; Agarwal, A.; Khasa, S. Electrical characterization of lithium bismuth borate glasses containing cobalt/vanadium ions. Solid State Ion. 2017, 312, 21–31.
51. Środa, M.; Świontek, S.; Gieszczyk, W.; Bilski, P. The effect of lithium fluoride on the thermal stability and thermoluminescence properties of borosilicate glass and glass-ceramics. J. Eur. Ceram. Soc. 2020, 40, 472–479.
52. Puchalska, M.; Bilski, P.; Olko, P. Thermoluminescence glow peak parameters for LiF:Mg,Ti with modified activator concentration. Radiat. Meas. 2007, 42, 601–604.
53. Divina, R.; Sathiyapriya, G.; Marimuthu, K.; Askin, A.; Sayyed, M. Structural, elastic, optical and γ-ray shielding behavior of Dy3+ ions doped heavy metal incorporated borate glasses. J. Non-Cryst. Solids 2020, 545, 120269.
54. Mahmoud, K.A.; Tashlykov, O.L.; Sayyed, M.I.; Kavaz, E. The role of cadmium oxides in the enhancement of radiation shielding capacities for alkali borate glasses. Ceram. Int. 2020, 46, 23337–23346.
55. Sadeq, M.S.; Abdo, M.A. Effect of iron oxide on the structural and optical properties of alumino-borate glasses. Ceram. Int. 2021, 47, 2043–2049.
56. Abouhaswa, A.S.; Sayyed, M.I.; Mahmoud, K.A.; Al-Hadeethi, Y. Direct influence of mercury oxide on structural, optical and radiation shielding properties of a new borate glass system. Ceram. Int. 2020, 46, 17978–17986.
57. Liu, J.; Yang, K.; Zhai, J.; Shen, B. Effects of crystallization temperature on phase evolution and energy storage properties of BaO-Na2O-Nb2O5-SiO2-Al2O3 glass-ceramics. J. Eur. Ceram. Soc. 2018, 38, 2312–2317.
58. Sigel, G.H.; Ginther, R.J. Effect of iron on ultraviolet absorption of high purity soda-silica glass. Glass Technol. 1968, 9, 66.
59. Duffy, J.A. Ultraviolet transparency of glass: A chemical approach in terms of band theory, polarisability and electronegativity. Phys. Chem. Glasses 2001, 42, 151–157.
60. Abdelghany, A.M.; ElBatal, H.A.; EzzElDin, F.M. Influence of CuO content on the structure of lithium fluoroborate glasses: Spectral and gamma irradiation studies. Spectrochim. Acta Part A Mol. Biomol. Spectrosc. 2015, 149, 788–792.
61. Abdelghany, A.M.; ElBatal, H.A. Optical and μ-FTIR mapping: A new approach for structural evaluation of V2O5-lithium fluoroborate glasses. Mater. Des. 2016, 89, 568–572.

62. Koo, J.; Bae, B.S.; Na, H.K. Raman spectroscopy of copper phosphate glasses. J. Non-Cryst. Solids 1997, 212, 173–179.
63. Ruiz-Aguilar, C.; Alcántara-Quintana, L.E.; Aguilar-Reyes, E.A.; Olivares-Pinto, U. Fabrication, characterization, and in vitro evaluation of β-TCP/ZrO2-phosphate-based bioactive glass scaffolds for bone repair. Boletín De La Soc. Es Pañola De Cerámica Y Vidr. 2020, 1–12.
64. Sekha, A.V.; Pavić, L.; Moguš-Milanković, A.; Purnachand, N.; Reddy, A.S.S.; Raju, G.N.; Veeraiah, N. Dielectric characteristics, dipolar relaxation dynamics and ac conductivity of CuO added lithium sulpho-phosphate glass system. J. Non-Cryst. Solids 2020, 543, 120157.
65. Liu, C.-X.; Pan, H.; Lv, J.-Y.; Chen, J.-Y.; Lin, S.-B.; Zheng, R.-L.; Fu, L.-L.; Zhang, L.-L. An infrared 2D Nd3+-doped phosphate glass waveguide formed by proton implantation and femtosecond laser ablation. Infrared Phys. Technol. 2021, 113, 103578.
66. Prasad, S.; Reddy, M.S.; Kumar, V.R.; Veeraiah, N. Specific features of photo and thermoluminescence of Tb3+ ions in BaO–M2O3 (M = Ga, Al, In)–P2O5 glasses. J. Lumin. 2007, 127, 637–644.
67. Wahab, E.A.; El-Maaref, A.; Shaaban, K.; Börcsök, J.; Abdelawwad, M. Lithium cadmium phosphate glasses doped Sm3+ as a host material for near-IR laser applications. Opt. Mater. 2021, 111, 110638.
68. Murashov, A.; Sidorov, A.; Stolyarchuk, M.; Boiko, M. Effect of X-ray irradiation and thermal treatment on luminescent properties of barium-phosphate glasses doped with silver and copper. J. Non-Cryst. Solids 2017, 477, 1–6.
69. Hirano, S.; Kawano, N.; Okada, G.; Kawaguchi, N.; Yanagida, T. PL and TSL properties of tin-doped zinc sodium phosphate glasses. Radiat. Meas. 2018, 112, 16–20.
70. Ivascu, C.; Gabor, A.T.; Cozar, O.; Daraban, L.; Ardelean, I. FT-IR, Raman and thermoluminescence investigation of P2O5–BaO–Li2O glass system. J. Mol. Struct. 2011, 993, 249–253.
71. Elisa, M.; Iordache, S.-M.; Vasiliu, I.; Grigorescu, C.; Sava, B.; Boroica, L.; Filip, A.; Dinca, M.; Bartha, C.; de Acha, N.; et al. Peculiarities of the structural and optical properties of rare-earth-doped phosphate glasses for temperature sensing applications. J. Non-Cryst. Solids 2021, 556, 120569.
72. Manchester, R.A.; Todorova, T.Z.; Werner-Zwanziger, U. Mixture designs to investigate the role of alkali and alkaline earth cations on composition-structure-property relationships in ternary borate glass networks. J. Non-Cryst. Solids 2021, 569, 120982.
73. Pugliese, D.; Veber, A.; Lemière, A. Effect of post-heat-treatment on the structural, spectroscopic and dissolution properties of a highly stable Er3+-doped multi-component phosphate glass. J. Alloys Compd. 2021, 883, 160878.

74. Akyildirim, H.; Kavaz, E.; El-Agawany, F.I. Radiation shielding features of zirconolite silicate glasses using XCOM and FLUKA simulation code. J. Non-Cryst. Solids 2020, 545, 120245.
75. Kilic, G.; Ilik, E.; Issa, S.A.M. Ytterbium (III) oxide reinforced novel TeO2–B2O3–V2O5 glass system: Synthesis and optical, structural, physical and thermal properties. Ceram. Int. 2021, 47, 18517–18531.